Chemistry–A European Journal
Research Article
doi.org/10.1002/chem.202200267
Chemistry Europe
European Chemical Societies Publishing
www.chemeurj.org

# Photoswitching Affinity and Mechanism of Multivalent Lectin Ligands

Uwe Osswald,[a] Johannes Boneberg,[b] and Valentin Wittmann*[a]

**Abstract:** Multivalent receptor–ligand binding is a key principle in a plethora of biological recognition processes. Immense binding affinities can be achieved with the correct spatial orientation of the ligands. Accordingly, the incorporation of photoswitches, which can be used to reversibly change the spatial orientation of molecules, into multivalent ligands is a means to alter the binding affinity and possibly also the binding mode of such ligands. We report a divalent ligand for the model lectin wheat germ agglutinin (WGA) containing an arylazopyrazole photoswitch. This switch, which has recently been introduced as an alternative to the more commonly used azobenzene moiety, is characterized by almost quantitative *E*/*Z* photoswitching in both directions, high quantum yields, and high thermal stability of the *Z* isomer. The ligand was designed in a way that only one of the isomers is able to bridge adjacent binding sites of WGA leading to a chelating binding mode. Photoswitching induces an unprecedentedly high change in lectin binding affinity as determined by isothermal titration calorimetry (ITC). Furthermore, additional dynamic light scattering (DLS) data suggest that the binding mode of the ligand changes from chelating binding of the *E* isomer to crosslinking binding of the *Z* isomer.

## Introduction

Carbohydrates as parts of glycoconjugates, such as glycoproteins or glycolipids, are indispensable moieties in many cell biological recognition processes.[1] Because individual carbohydrate epitopes interact only weakly with their protein receptors, the concept of multivalency is a key principle used in nature to achieve the required high affinity in such processes.[2] The observation, that the presentation and orientation of carbohydrate moieties are decisive for an effective multivalent interaction, dates back to the seminal work of Lee in the 1970s.[3] Accordingly, a plethora of scaffolds have been employed to construct tailored multivalent carbohydrate ligands that can effectively interact with carbohydrate-binding proteins termed lectins thereby achieving strongly improved binding affinities (avidities).[4] Screening of combinatorial libraries of spatially diverse glycoclusters provides an alternative approach to perfectly fitting lectin ligands.[5]

Among the different binding modes of multivalent interactions, chelating binding, that is, the bridging of adjacent binding sites by a multivalent ligand, is assumed to make a major contribution to high affinity binding.[6] Especially for less flexible ligands, even small deviations of the perfect structure significantly decrease affinity.[7] Therefore, control of the mode of presentation and orientation of carbohydrate moieties provides a possible mode of regulation of these recognition processes both in biological as well as in synthetic systems. A proven and widely applied method to induce changes in orientation of structures on demand is the application of photoswitches.[8] A prime example are azobenzene photoswitches that have also found some application in glycosciences.[9] High spatiotemporal control and a clean and reversible reaction that can be cycled many times are typical for the class of azobenzene photoswitches. Among the disadvantages of azobenzene photoswitches are, however, incomplete photoswitching in the photo stationary state (PSS) due to overlapping absorption bands of the *E* and *Z* isomers and a limited thermal stability of the *Z* isomer leading to isomerization to the thermodynamically favored *E* isomer. Recently, arylazopyrazoles (Scheme 1A) have been introduced as a new class of photoswitches that offer almost quantitative *E*/*Z* photoswitching in both directions and high thermal stability of the *Z* isomer.[10] Arylazopyrazoles have been incorporated, for example, into amidohydrolase inhibitors,[11] neuropeptide Y receptor ligands,[12] and a mitotic kinesin inhibitor.[13] However, they have not yet been used for the construction of photoswitchable lectin ligands.

Jayaraman pioneered the field of photoswitchable multivalent carbohydrate ligands[14] and reported the synthesis of up to octavalent galactose and lactose clusters containing amide-substituted azo-benzene moieties.[15] In the PSS of the ligands,

[a] U. Osswald, Prof. Dr. V. Wittmann
Department of Chemistry, University of Konstanz
78457 Konstanz (Germany)
E-mail: mail@valentin-wittmann.de
[b] Prof. Dr. J. Boneberg
Department of Physics, University of Konstanz
78457 Konstanz (Germany)

Supporting information for this article is available on the WWW under https://doi.org/10.1002/chem.202200267

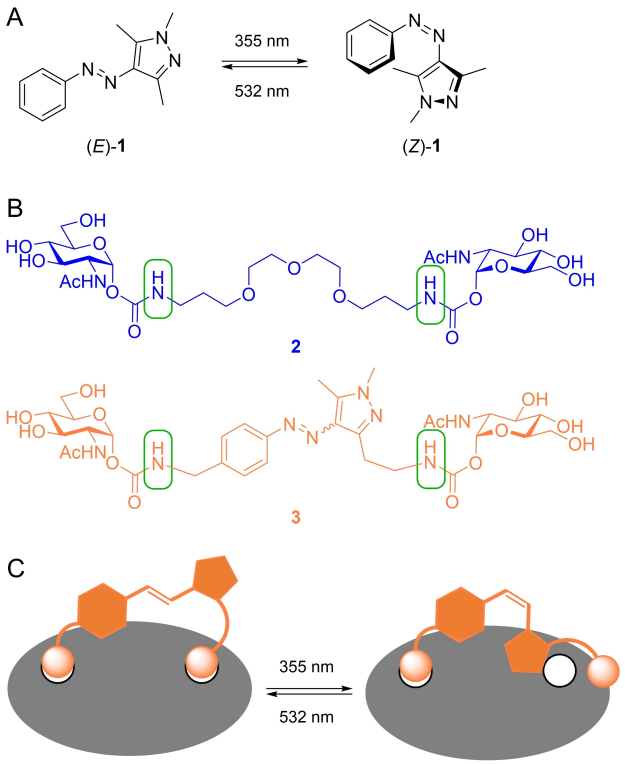


**Scheme 1.** A) Photoisomerization of arylazopyrazole **1**. B) Divalent WGA ligand **2**, which is able to bridge adjacent binding sites of WGA, and photoswitchable divalent ligand **3** obtained from molecular modeling. C) Schematic representation of the effect of *E*/*Z* isomerization of photoligand **3** on WGA binding. Sugar epitopes represented as orange spheres and WGA binding sites as white circles.

the *Z* isomer reached proportions up to 70%, and binding studies by isothermal titration calorimetry (ITC) uncovered photoinduced differences in binding affinities. However, since the clusters were not able to bridge binding sites within the used lectins PNA and ConA, respectively, the origin of the different $K_d$ values was not clear and crosslinking was proposed to be involved which was in line with the observation of precipitation.

In 2014, the Hartmann group reported di- and trivalent Gal-(and Man-)containing glycooligomers with one and two azo-benzene switches.[16] In the PSS, up to 80% of the *Z* isomer were detected. Using surface plasmon resonance (SPR), $IC_{50}$ values for the inhibition of the binding of the lectin PA-IL to galactose-modified chip surfaces were determined. Upon photoswitching, the $IC_{50}$ values varied by a factor of up to 1.6 as observed for the divalent ligand. Structural models showed that the distance between the sugar moieties was much longer than the distance of the lectin binding sites independent of the configuration of the azo-benzene switches, allowing a chelating binding mode for both isomers.

The Lindhorst group extensively studied the synthesis and photochromic properties of mono-, di-, and trivalent carbohydrate-substituted azo-benzene derivatives.[17] It was found that the substitution pattern of the azo-benzene moiety strongly influences the PSS and thermal stability of the *Z* isomer. Soluble monovalent mannose-substituted azo-benzene derivatives were investigated for their potency to inhibit the adhesion of type 1-fimbriated *Escherichia coli* to mannan-coated microtiter plate surfaces.[18] Although this experimental setup did not lead to different $IC_{50}$ values for the *E* and *Z* isomers, immobilization of glycosylated azo-benzene derivatives on microtiter plates[19] or human cell membranes[20] resulted in photoswitchable surfaces that showed marked differences in bacterial adhesion, dependent on the light-induced configuration of the glycosylated azo-benzene moiety. These findings underline the significance of orientation of carbohydrate ligands for efficient multivalent recognition by lectins.

Although photoswitchable lectin ligands have been reported as exemplified above, an example of a ligand with only one of the two photoisomers being able to bridge adjacent binding sites of a multivalent lectin is so far unknown. Here, we report the first example of such a photoswitchable lectin ligand. As switching element within the divalent ligand, we chose the recently developed arylazopyrazole moiety that resulted in almost quantitative photoisomerization between the *E* and *Z* configuration with high quantum yields and a long thermal half-life of the *Z* isomer. As expected, the ligand shows unprecedentedly high differences in binding affinity upon photoswitching as determined by ITC. Furthermore, we discovered a change of the binding mode after *E*/*Z* isomerization.

## Results and Discussion

### Ligand design

To obtain a photoswitchable divalent ligand with an unprecedentedly high photoinducible effect on the binding affinity, we selected a lectin with short distances between the binding sites, as we expected that subtle changes of the linker geometry would have a large impact on the binding affinity. Wheat germ agglutinin (WGA),[21] which has been extensively examined by us in the past,[22] is a well-suited example. At neutral pH, two monomers form a stable homodimer with $C_2$ symmetry and a mass of 34 kDa.[23] The dimer exhibits eight carbohydrate binding sites which are grouped in pairs and located at the interface of the two monomers, with a shortest distance of 14 Å between the binding sites (distance between anomeric oxygens).[22b,23–24] WGA contains two types of binding sites, four so-called primary binding sites with higher affinity and four secondary binding sites with lower affinity. All binding sites show affinity to *N*-acetylglucosamine and oligomers thereof, however, the secondary sites have been reported to bind too weakly to be detected in solution.[25] According to an X-ray structure analysis, the previously reported divalent ligand **2** (Scheme 1B) is able to bridge pairs of primary binding sites.[22b] Starting from this structure (PDB ID: 2X52), we manually screened for a linker containing a photoswitchable arylazopyrazole unit that is able to connect the two carbamate nitrogens of **2** (highlighted in green in Scheme 1B). Different substitution patterns of arylazopyrazole **1** were modeled and the 3D linker geometries were optimized by MM2 forcefield calculations.

Both *E* as well as *Z* configured arylazopyrazole units were modeled to identify differences in their ability to bridge the two carbamate nitrogens of **2** which was expected to result in different binding affinities of the divalent ligand. The optimized structures were superimposed with divalent ligand **2** in the crystal structure by adjusting the single bond dihedral angles. As a result, divalent photoligand **3** shown in Scheme 1B was obtained. This ligand can bridge two GlcNAc binding sites when existing in the *E* configuration whereas a strain-free chelating binding mode is not possible for the *Z* isomer (Scheme 1C and Figure 1). Accordingly, we expected a high difference in binding affinity for the two photoisomers.

## Synthesis

The first building block required for the synthesis of photo ligand **3** was enaminone **6** (Scheme 2). Although **6** is a literature-known compound,[26] a feasible synthetic route had to be established, as the compound was only observed as rearrangement product of a complex isoxazoline-5-spiro derivative. Niphakis et al. published a general method for the synthesis of six- and seven-membered cyclic enaminones[27] which was modified to obtain a short and high yielding synthetical route to **6**. Weinreb amide **4**[27] was substituted with propyn-1-yl magnesium bromide to yield novel ynone **5**. Boc deprotection and subsequent base-induced cyclization gave enaminone **6**.

Next, Fmoc-protected aniline derivative **8** was synthesized from benzylamine **7** according to a modified literature procedure[28] (Scheme 3). Subsequent azo coupling with enaminone **6** gave azo intermediate **9**. The conversion to arylazopyrazoles and simultaneous Fmoc deprotection was achieved by refluxing with methylhydrazine in EtOH. To facilitate subsequent separation of the isomers, the primary amines were Boc protected. Both arylazopyrazoles **10** and **11** were obtained as mixtures of *E* and *Z* isomers. Since we observed that separation of the *E* isomers (*E*)-**10** and (*E*)-**11** was more convenient (see the Supporting Information for HPLC profiles), we irradiated the mixture with green laser light (532 nm, 1 W, 6 min) to isomerize both compounds to their *E* form. After RP-HPLC, arylazopyrazoles (*E*)-**10** and (*E*)-**11** were obtained in a ratio of 57:43 and a combined yield of 44% from **9**. Assignment of the two isomers was possible by HMBC NMR spectroscopy taking the indicative $^{2}J$ and $^{3}J$ heteronuclear couplings shown in Scheme 3 into account.

With the novel arylazopyrazoles (*E*)-**10** and (*E*)-**11** in hand, synthesis of a functional WGA ligand was performed. We expected no difference between both regioisomers in terms of

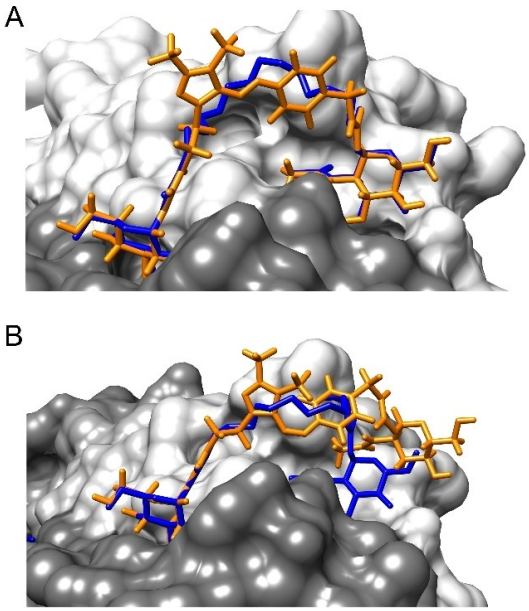


**Figure 1.** Results of crystal structure modeling. Depicted in light and dark gray are the WGA monomers in complex with ligand **2** in blue (PDB ID: 2X52). A) Manually optimized conformation of photoligand (*E*)-**3** (orange) superimposed on ligand **2** in a chelating binding mode. B) For photoligand (*Z*)-**3**, no conformation allowing a strain-free chelating binding was found.

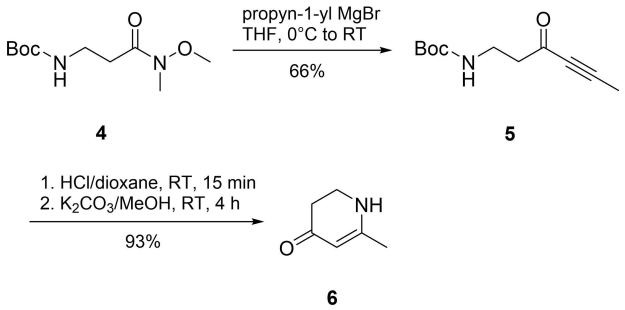


**Scheme 2.** Synthesis of enaminone **6.**

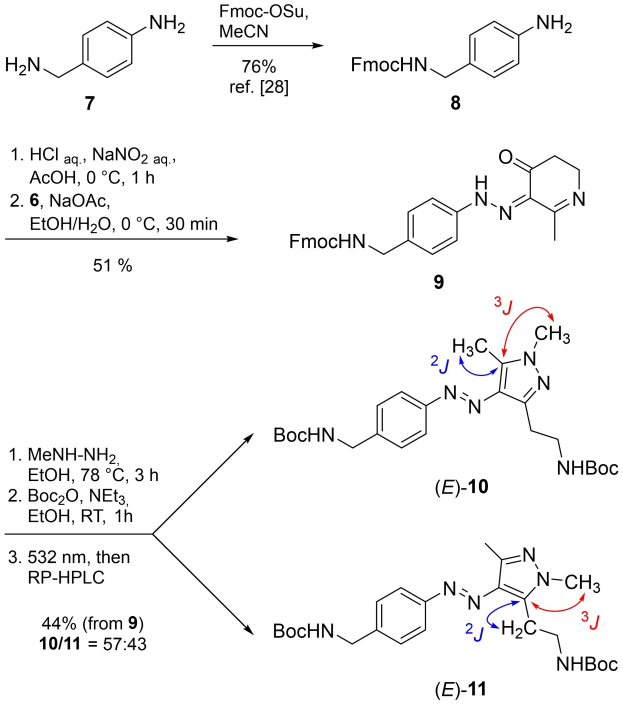


**Scheme 3.** Preparation of arylazopyrazoles **10** and **11** as pure *E* isomers.

photoisomerization properties and binding behavior to WGA. Therefore, we proceeded with the purified major isomer (*E*)-**10**. To maintain the *E* configuration facilitating isolation and characterization of products, we continued the synthesis from here on under nearly total darkness although synthesis under ambient light was also possible and, due to easier handling, provided higher yields. Arylazopyrazole (*E*)-**10** was deprotected with TFA and subsequently functionalized with literature-known carbonate **12**[22b,29] (Scheme 4). The obtained purified photoglycoconjugate **13** was then deacetylated with potassium carbonate in methanol to yield the ligand (*E*)-**3** without the need for further purification.

### Photoisomerization properties and thermal half-life

Photoisomerization properties of photoligand **3** were investigated by UV/vis spectroscopy coupled with laser irradiation (Figure 2A). To obtain a defined starting point, the sample was irradiated with high intensity 532 nm light until the photo stationary state with predominantly *E* configuration was reached. Then the wavelength was changed to 355 nm to trigger switching from *E* to *Z* configuration and spectra were recorded after increasing irradiation times until no more changes occurred and the photo stationary state with predominantly *Z* configuration was reached (Figure 2B). The procedure was repeated for the reverse switching process (Figure 2C). The obtained spectra exhibit several well defined isosbestic points (e.g., at 240 and 298 nm) indicating that no side reactions had

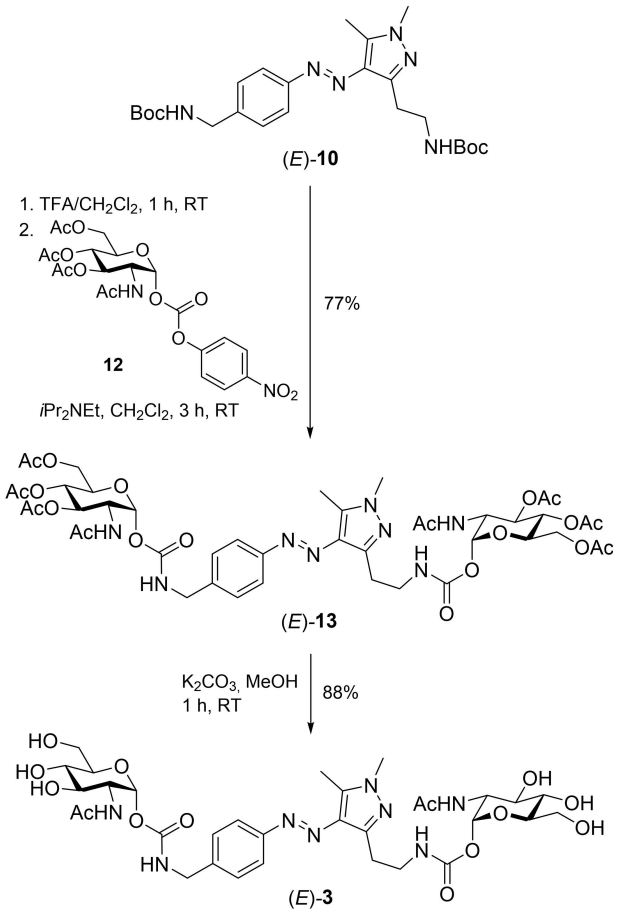


**Scheme 4.** Synthesis of photoligand (*E*)-**3**.

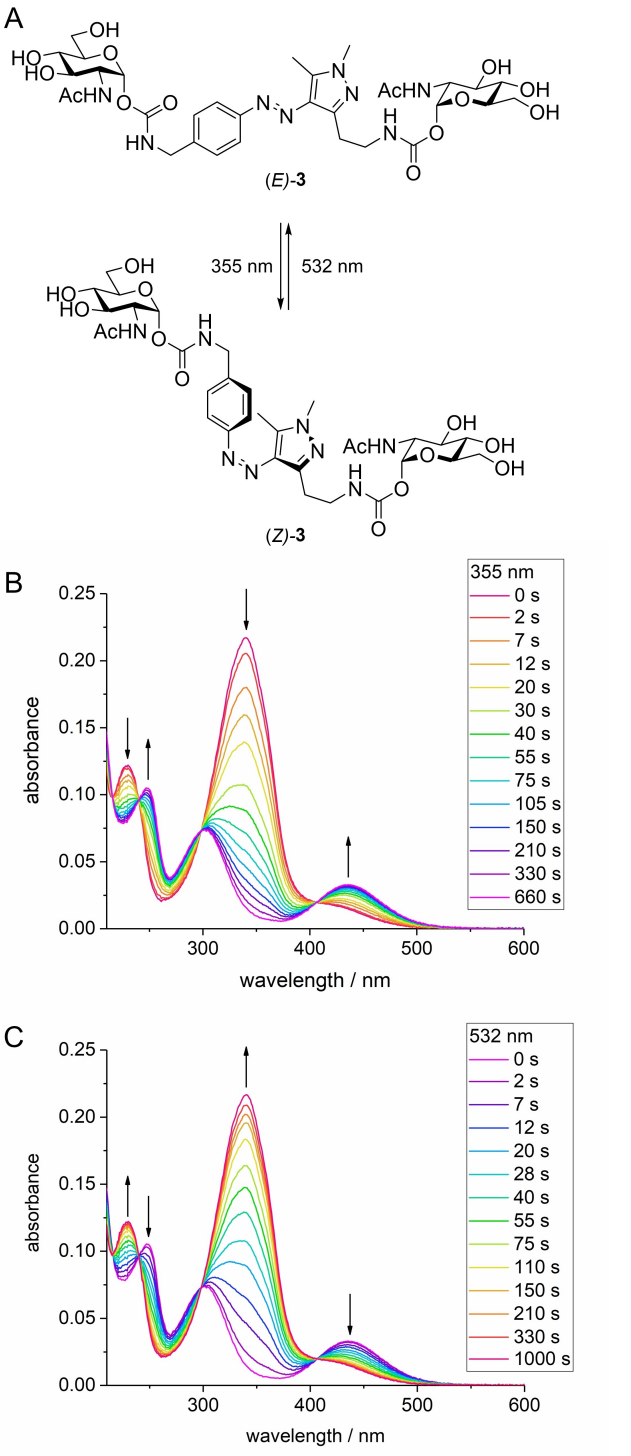


**Figure 2.** A) Photoswitching of arylazopyrazole **3**. Irradiation time-dependent UV/vis spectra of photoligand **3** in water depicting the switching processes upon irradiation at B) 355 nm, 10 Hz, 86.5 μJ and C) 532 nm, 10 Hz, 4.45 mJ.

occurred during the switching processes. The composition of the photo stationary states in water was determined by RP-HPLC and integration of the UV/vis signals at the two isosbestic points mentioned (chromatograms shown in the Supporting Information). We found almost quantitative (97%) switching in both directions which is comparable to the reported value of the scaffold molecule **1**.[10a]

Next, we determined quantum yields for the photochemical switching processes of the photo glycoconjugate **3**. As a reference, we also investigated the previously published[10a] unsubstituted photoswitch **1**. Quantum yields were determined from the irradiation-time-dependent UV/vis spectra[10a] as described in the Supporting Information. The obtained values are listed in Table 1.

The quantum yields of photoswitch **1** previously have been determined in acetonitrile.[10a] Therefore, we repeated this experiment and, additionally, used water as solvent. Interestingly, the $E \rightarrow Z$ process became more efficient in water while the efficiency of the $Z \rightarrow E$ process slightly decreased, showing the influence of solvation on photochemical processes. The same effect has also been observed for azobenzene derivatives.[30] In this case, the sum of quantum yields ($\Phi_{E\rightarrow Z} + \Phi_{Z\rightarrow E}$) remained almost constant in acetonitrile and water/ethanol. In case of arylazopyrazole **1**, however, the sum of the quantum yields ($\Phi_{E\rightarrow Z} + \Phi_{Z\rightarrow E}$) increased in aqueous solution.

The quantum yields of photoligand **3** were determined in water allowing to estimate the effects of the substitution with the two GlcNAc moieties. Compared to the unsubstituted photoswitch **1**, the quantum yield of the $E \rightarrow Z$ process decreased from 0.70 to 0.52 whereas the value of the $Z \rightarrow E$ process increased significantly from 0.48 to 0.78. The observation that the switching process from the *Z* isomer to the *E* isomer is more efficient for the substituted photoligand **3** might be explained by the increased steric demand of the carbohydrate substituents. Gratifyingly, the quantum yields were still very high (or even higher) after modification of the methyl group in the 3-position of the pyrazole. In contrast, modification of the NMe group of the pyrazole has been observed to significantly decrease quantum yields.[10b]

Subsequently, we evaluated the thermal half-life by UV/vis spectroscopy. We found that photoligand (*Z*)-**3** relaxes very slowly in water at a temperature of 20 °C with an estimated half-life of 29.4 ± 0.7 days (see the Supporting Information for details). Having determined the photochemical properties of the novel photoligand **3**, we proceeded with the quantification of its WGA binding behavior.

**Table 1.** Quantum yields $\Phi$ for the switching from $E \rightarrow Z$ (irradiation at 355 nm) and $Z \rightarrow E$ (irradiation at 532 nm) at 25 °C.

| Compound | Solvent | $\Phi_{E\rightarrow Z}$ (355 nm) | $\Phi_{Z\rightarrow E}$ (532 nm) |
|---|---|---|---|
| **1** | MeCN | 0.46 ± 0.04 | 0.56 ± 0.05 |
| **1** | $H_2O$ | 0.70 ± 0.08 | 0.48 ± 0.05 |
| **3** | $H_2O$ | 0.52 ± 0.07 | 0.78 ± 0.08 |

## WGA binding affinity

Next, we determined the binding affinities of both isomers of photoligand **3** to the plant lectin WGA by ITC. ITC is a well-established method that provides the stoichiometry and thermodynamic characterization of protein-ligand interactions and has been widely used to study the binding of (multivalent) carbohydrates to lectins[31] including WGA.[22d,f,32] Small aliquots of **3** dissolved in phosphate buffer (pH 7) containing 5% DMSO to ensure solubility were irradiated with light of either 532 or 355 nm until the PSS was reached. The subsequent ITC experiments were performed in darkness. In each case, three independent experiments were carried out (see the Supporting Information). Raw and integrated data of representative experiments are depicted in Figure 3. The obtained binding parameters for both isomers of photoligand **3** are listed in Table 2. It is worth mentioning that the presence of 3% of the minor isomer within the PSS of both samples results in only small deviations of the $K_d$ values that are fully within the standard deviations of the $K_d$ values given in Table 2 (cf. Supporting Information). As expected from our initial design, the *E* isomer has a significantly higher WGA binding affinity than the *Z* isomer. The $K_d$ of isomer (*E*)-**3** (0.177 μM) is comparable to that of the best divalent ligand reported so far (compound **2**: $K_d = 0.102$ μM[22f]). The

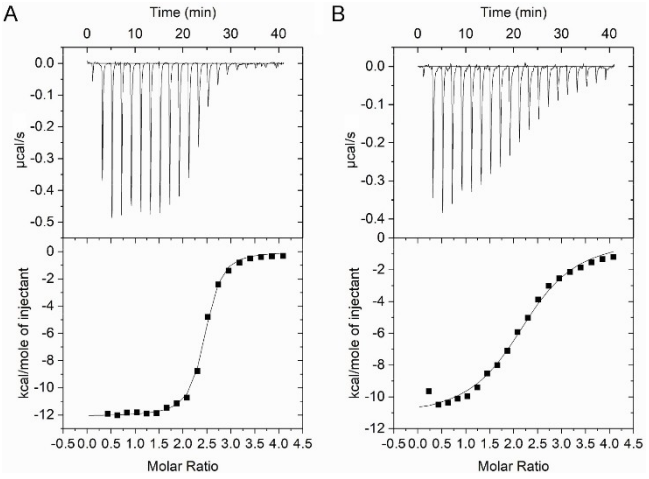


**Figure 3.** Representative thermograms obtained by ITC for the binding of isomers A) (*E*)-**3** and B) (*Z*)-**3** to WGA in phosphate buffer (pH 7) containing 5% DMSO at 25 °C.

**Table 2.** ITC-derived thermodynamic WGA-binding parameters determined for ligand **3** in *E* and *Z* configuration at pH 7 and 25 °C. Standard deviation obtained from three independent experiments.

| Compound | $n$[a] | $\Delta H°$ [kcal mol$^{-1}$] | $-T\Delta S°$ [kcal mol$^{-1}$] | $K_d$ [μM] |
|---|---|---|---|---|
| (*E*)-**3** | 2.46 ± 0.2 | −12.32 ± 0.33 | 3.13 ± 0.48 | 0.177 ± 0.053 |
| (*Z*)-**3** | 2.15 ± 0.2 | −12.32 ± 0.72 | 4.60 ± 0.74 | 2.21 ± 0.08[b] |

[a] Binding stoichiometry (ligand to protein ratio) referred to WGA homodimer; [b] The $K_d$ of (*Z*)-**3** is reported as "apparent $K_d$" because it includes the formation of a 2:4 complex according to the DLS experiments described below.

stoichiometry of binding is approximately 2 in agreement with only the two pairs of primary binding sites being occupied. Remarkably, upon switching to the *Z* configuration, the $K_d$ increased by a factor of 12.5 to a value of 2.21 μM, thus indicating significantly declined binding affinity. This is, to the best of our knowledge, the highest photoswitch-induced effect in carbohydrate lectin interaction reported to date.

Interestingly, both isomers have the same binding enthalpy $\Delta H^\circ$; this indicates that for both ligands both GlcNAc moieties are involved in binding. The observed difference in binding affinity is exclusively caused by different binding entropies $\Delta S^\circ$. In addition, both isomers have a comparable binding stoichiometry. A possible explanation for these results, that considers the fact that isomer (*Z*)-**3** is not able to bridge adjacent binding sites of a single WGA dimer, could be the cross linking of WGA dimers. In this respect, it is worth mentioning that we did not observe any precipitate formation upon addition of either (*Z*)-**3** or (*E*)-**3**. To detect the possible formation of oligomers, we employed dynamic light scattering (DLS), as this method previously allowed the detection of ligand-WGA complexes.[22d,f]

### Detection of ligand-induced protein oligomerization

WGA solutions were incubated with two equivalents of either isomer (*E*)-**3** or (*Z*)-**3** and then investigated by DLS. As a control, a solution of WGA alone was used. Figure 4 depicts the mean hydrodynamic radii determined from the intensity distributions shown in the Supporting Information as well as the molecular weights calculated thereof. For the solution of WGA alone, a mean hydrodynamic radius of 2.70 nm was determined. From this value, a molecular weight of 34 kDa was calculated which is in very good agreement with the molecular weight of WGA. The calculated molecular weight of WGA in complex with (*E*)-**3** slightly increased to 42 kDa indicating the absence of oligomer formation. In case of WGA in complex with isomer (*Z*)-**3**, which is not able to bind in a chelating binding mode, we observed a strong increase of the calculated molecular weight to 79.3 kDa. The doubling of molecular weight is in agreement with a crosslinking binding mode. Taking the binding stoichiometry determined by ITC into account, the formation of a complex consisting of two WGA dimers and four molecules of ligand (*Z*)-**3** is reasonable. According to molecular modelling, such a 2:4 complex is indeed possible (see the Supporting Information). This binding mode is further supported by the stronger unfavorable binding entropy of isomer (*Z*)-**3** determined by ITC because the formation of a complex of six molecules is linked to a severe loss of translational degrees of freedom.

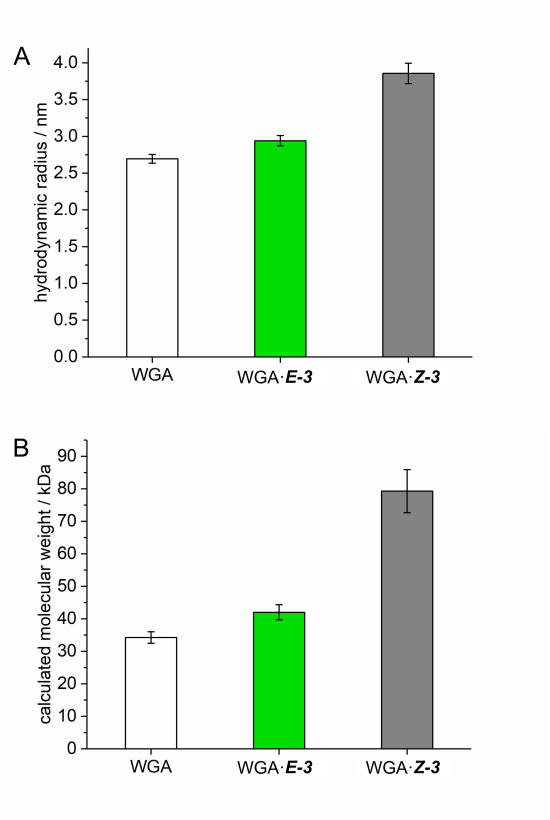


**Figure 4.** Results of DLS experiments in phosphate buffer with 5% DMSO. A) Mean hydrodynamic radii *r* (derived from intensity distributions of five measurements shown in the Supporting Information) of species present in solutions of WGA (white) and WGA with added photoligands (*E*)-**3** (green) and (*Z*)-**3** (gray) after filtration through a 100 nm cutoff filter. B) Molecular masses of the species calculated from the hydrodynamic radii shown in (A) by using the protein size mode of Zetasizer software v7.12.

## Conclusions

In summary, we have presented the first arylazopyrazole-based photoswitchable divalent lectin ligand for which only one of the isomers is able to bridge adjacent binding sites of the lectin. The ligand is characterized by almost quantitative switching in both directions, high quantum yields for both switching processes, and a very high thermal half-life of one month. With WGA as a model protein, an unprecedentedly high effect of photoswitching on binding affinity was determined by ITC. DLS experiments revealed a strong difference in hydrodynamic radii for WGA–ligand complexes of the *E* and *Z* isomers of the novel photoligand. This indicates that a photoswitch-induced change from a chelating to a crosslinking binding mode occurred and exemplifies the numerous options for regulating biological recognition processes through multivalency. A system allowing a reversible photo-responsive change of binding modes could also be used in smart soft materials for adjusting chain crosslinking within networks. Quantitative light-induced control over ligand geometry might be a useful tool for the development of novel capture-and-release glycoarrays or future materials for lectin purification.

## Experimental Section

### General methods

All reactions were monitored by TLC on silica gel 60 F254 (Merck) on aluminum sheets with detection by UV light ($\lambda = 254$ nm, 366 nm). Depending on the compound, either acidic ethanolic *p*-anisaldehyde solution, acidic aqueous potassium permanganate solution, or aqueous butanolic ninhydrin solution, followed by gentle heating, was additionally used for visualization. Preparative flash chromatography (FC) was performed manually with silica 60 M from Macherey-Nagel. NMR spectra were recorded at RT on Avance III 400 and Avance III 600 instruments from Bruker. Chemical shifts are reported relative to solvent signals ($CDCl_3$: $\delta_H = 7.26$, $\delta_C = 77.16$; [$D_6$]DMSO: $\delta_H = 2.50$, $\delta_C = 39.52$; $CD_3OD$: $\delta_H = 3.31$, $\delta_C = 49.00$). High-resolution mass spectra (HRMS) were recorded on a Bruker micrOTOF II instrument with electrospray ionization in acetonitrile and water with 0.1% TFA. Semi-preparative high-pressure liquid chromatography (HPLC) was performed on a LC-20A prominence system (pumps LC-20AT, auto sampler SIL-20 A, column oven CTO-20AC, diode array detector SPD–M20A, ELSD-LT II detector, controller CBM-20 A and software LC-solution) from Shimadzu with a Kinetex 5 µm $C_{18}$ 100 Å column (250×21.2 mm, flow 9 mL min$^{-1}$) from Phenomenex. Analytical high-performance liquid chromatography-mass spectrometry (LC–MS) was performed on a LC/MS-2020 system from Shimadzu (high pressure pumps LC-20AD, auto sampler SIL-20AT HAT, column oven CTO-20AC, UV-vis detector SPD-20 A, communication bus module CBM-20 A, LC/MS-2020 ESI detector and LC–MS solution software) with a Kinetex 2.6 µm $C_{18}$ 100 Å column (150×4.60 mm, flow 0.4 mL min$^{-1}$) from Phenomenex. On both systems a binary gradient of acetonitrile in water (without formic acid) was used.

***tert*-Butyl (3-oxohex-4-yn-1-yl)carbamate (5)**: Weinreb amide **4**[27] (1.10 g, 4.74 mmol) was dissolved in anhydrous THF (300 mL) under $N_2$ atmosphere and cooled to 0 °C followed by dropwise addition of a 0.5 M propyn-1-yl magnesium bromide solution (47.4 mL, 23.68 mmol). The mixture was allowed to warm up to RT while being monitored by TLC. As soon as TLC showed nearly full conversion, the reaction mixture was quenched by careful addition of 10% HCl solution (50 mL). It was stirred for another 10 min followed by dilution with water and extraction with ethyl acetate (3×60 mL). The combined organic phases were washed with $NaHCO_3$ dried over $Na_2SO_4$, filtrated, and solvents were removed under reduced pressure. The obtained crude mixture was purified by FC (light petroleum (PET)/EtOAc 4:1 to 1:1) yielding ynone **5** (0.66 g, 66%) as a colorless oil. $R_f = 0.51$ (PET/EtOAc 1:1); $^1$H NMR ($CDCl_3$, 400 MHz): $\delta = 4.91$ (br s, 1 H, NH), 3.40 (q, $J = 5.9$ Hz, 2 H, $NCH_2$), 2.76 (t, 2 H, $J = 5.8$ Hz, $CH_2C(O)$), 2.02 (s, 3 H, $C{\equiv}CCH_3$), 1.42 (s, 9 H, $C(CH_3)_3$); $^{13}$C NMR ($CDCl_3$, 101 MHz): $\delta = 186.9$ (C=O), 155.9 (O(C=O)N), 91.3 (C≡), 80.2 (≡C–Me), 79.5 ($\underline{C}(Me)_3$), 45.6 ($CH_2$), 35.3 ($CH_2N$), 28.5 ($C(\underline{C}H_3)_3$), 4.2 (≡C–$\underline{C}H_3$); HRMS: m/z calcd. for $C_{11}H_{17}NO_3$: 212.1281 [$M$+H]$^+$, found: 212.1283.

**1-Aminohex-4-yn-3-one (6)**:[26] Ynone **5** (0.51 g, 2.41 mmol) was dissolved in 4 M HCl 1,4-dioxane solution (7.25 mL) and stirred for 15 min before volatile compounds were evaporated using a $N_2$ stream. The remaining solid was dried under reduced pressure for 15 min before it was dissolved in MeOH (240 mL). Potassium carbonate (1.67 g, 12.06 mmol) was added, and the mixture was stirred for 4 h. Upon concentration under reduced pressure, potassium salts started to precipitate and $CH_2Cl_2$ was added. The obtained mixture was filtered off and the filtrate was again concentrated. Precipitation and filtration steps were repeated once more before solvents were removed under reduced pressure. The crude mixture was purified by FC (EtOAc/MeOH 5:1) yielding enaminone **6** (0.25 g, 93%) as pale-yellow crystals. Characterization data were in full agreement with the previously reported data.[26]

**(9*H*-Fluoren-9-yl)methyl(4-aminobenzyl)carbamate (8)**:[28] Hünig's base (0.68 mL, 3.90 mmol) was added to a solution of 4-aminobenzylamine (**7**) (0.5 g, 4.09 mmol) in MeCN (5 mL) under a $N_2$ atmosphere and vigorous stirring. After cooling to 0 °C, a solution of Fmoc-OSu (1.31 g, 3.90 mmol) in MeCN (10 mL) was added dropwise over 10 min. Within a short time, a suspension started to form which was then allowed to warm up to RT over the course of 1 h. The mixture was diluted with water (25 mL) and ethyl acetate (60 mL). The organic phase was washed with brine (25 mL), dried over $Na_2SO_4$, and concentrated under reduced pressure. The obtained crude product was purified by FC (PET/EtOAc 1.7:1 to 1:1) to obtain amine **8** (1.34 g, 76%) as an off-white solid. Characterization data were in full agreement with the previously reported data.[28]

**(9*H*-Fluoren-9-yl)methyl ((*Z*))-(4-(2-(2-methyl-4-oxo-5,6-dihydropyridin-3(4*H*)-ylidene)hydrazineyl)benzyl)carbamate (9)**: A solution of $NaNO_2$ (38 mg, 0.55 mmol) in water (0.3 mL) was added dropwise to a suspension of amine **8** (172 mg, 0.55 mmol) in a mixture of water (0.6 mL), ethanol (1.2 mL), AcOH (0.6 mL) and 12 M HCl (0.1 mL) at 0 °C. After 1 h of stirring, the solution was transferred into a freshly prepared solution of enaminone **6** (73 mg, 0.66 mmol) and NaOAc (226 mg, 2.75 mmol) in a mixture of ethanol (1.5 mL) and water (1 mL) at 0 °C. After another 30 min of stirring at 0 °C, $CH_2Cl_2$ (10 mL) and sat. $NaHCO_3$ solution (5 mL) were added. The phases were separated, and the aqueous phase was extracted with $CH_2Cl_2$ (3×15 mL). The combined organic phases were dried over $MgSO_4$ before they were concentrated yielding a red foam which was purified by FC (EtOAc/MeOH 25:1) yielding azo compound **9** (131 mg, 51%) as an orange solid containing small amounts of decomposition products. The product was found to be very sensitive to moisture and aqueous acidic solutions and was immediately used for the next step. $R_f = 0.19$ ($CH_2Cl_2$/MeOH 19:1); $^1$H NMR ($CDCl_3$, 600 MHz): $\delta = 14.10$ (br s, 1 H, N–NH), 7.76 (m, 2 H, $H^{Fl-4}$ $H^{Fl-5}$), 7.59 (m, 2 H, $H^{Fl-1}$ $H^{Fl-8}$), 7.49–7.27 (m, 8 H, $H^{Fl-2}$ $H^{Fl-7}$ $H^{Fl-3}$ $H^{Fl-6}$ $H^{Ar-1}$ $H^{Ar-2}$), 5.17 (m, 1H, C(O)–NH), 4.48 (d, $J = 6.7$ Hz, 2 H, $CH_2O$), 4.36 (d, $J = 5.8$ Hz, 2 H, C$\underline{H}_2$NH), 4.22 (t, $J = 6.7$ Hz, 1 H, $H^{Fl-9}$), 3.87 (m, 2H, O=C–$CH_2$), 2.65 (t, $J = 6.7$ Hz, 2 H, $CH_2N$≡), 2.33 (s, 3 H, $CH_3$); $^{13}$C NMR ($CDCl_3$, 151 MHz): $\delta = 195.2$ (C=O), 166.3 (HN–N=C), 156.6 (O(C=O)N), 144.0 ($C^{Fl-10}$ $C^{Fl-13}$), 141.5 ($C^{Fl-11}$ $C^{Fl-12}$, $C^{Ar}$–NH–N), 135.6 ($\underline{C}^{Ar}$–$CH_2$–NH), 128,9 ($HC^{Ar-1}$), 127.8 ($HC^{Fl-3}$ $HC^{Fl-6}$), 127.7 (MeC=N), 127.2 ($HC^{Fl-2}$ $HC^{Fl-7}$), 125.1 ($HC^{Fl-1}$ $HC^{Fl-8}$), 120.1 ($HC^{Fl-4}$ $HC^{Fl-5}$), 116.1 ($HC^{Ar-2}$), 66.8 (Fl-$CH_2O$), 47.5 ($HC^{Fl-9}$), 46.4 ($CH_2$(C=O)), 44.7 (Ar-$CH_2N$), 38.3 (=$NCH_2$), 21.8 ($CH_3$); HRMS: calcd. for $C_{28}H_{26}N_4O_3$: 467.2078 [$M$+H]$^+$, found: 467.2059.

***tert*-Butyl ((*E*))-(4-((3-(2-((*tert*-butoxycarbonyl)amino)ethyl)-1,5-dimethyl-1*H*-pyrazol-4-yl)diazenyl)benzyl)carbamate ((*E*)-10) and *tert*-Butyl ((*E*))-(4-((5-(2-((*tert*-butoxycarbonyl)amino)ethyl)-1,3-dimethyl-1*H*-pyrazol-4-yl)diazenyl)benzyl)carbamate ((*E*)-11)**: Azo compound **9** (155 mg, 0.33 mmol) was dissolved in EtOH (5 mL) under $N_2$, and methyl hydrazine (0.30 mL, 2.66 mmol) was added followed by heating to 78 °C. After 3 h, the mixture was concentrated under reduced pressure and the remaining residue was co-evaporated with EtOH. The crude mixture was dissolved in EtOH (7 mL) and $Et_3N$ (0.32 mL, 2.33 mmol) and di-*tert*-butyldicarbonate (363 mg, 1.66 mmol) was added. After 1 h, all volatile compounds were removed under reduced pressure, the remaining solid was dissolved in ethyl acetate (25 mL) and washed with water (20 mL). Phases were separated and the aqueous phase was extracted with ethyl acetate (3×5 mL). The pooled organic phases were washed with brine then dried over $MgSO_4$, filtrated, and concentrated under reduced pressure. The residue was purified by FC (PET/EtOAc 4:1 to 1:2). The obtained mixture was irradiated with 532 nm (6 min, 1 W) to switch the product to the *E* configuration and then purified by HPLC (65–80% MeCN in water over 15 min) to obtain separated constitutional isomers (*E*)-**10** (24%) and (*E*)-**11** (18%) and a small mixed fraction (2%; 68.5 mg, 44% total) as yellow solids. (*E*)-**10**: HPLC: $t_R = 12.881$ min (65–80% MeCN in water over 15 min); $^1$H NMR ($CD_3OD$, 600 MHz): $\delta = 7.76$ (m, 2 H, $HC^{Ar}$), 7.39 (m, 2 H, $HC^{Ar}$), 4.29 (s, 2 H, Ar–$CH_2N$), 3.79 (s, 3 H, $NCH_3$), 3.39 (t, $J = 6.5$ Hz, 2 H, $CH_2$-C$\underline{H}_2$N), 3.03 (t, $J = 6.5$ Hz, 2 H, C$\underline{H}_2$–$CH_2$N), 2.59 (s, 3 H, $CH_3$), 1.47 (s, 9 H, $C(CH_3)_3$), 1.38 (s, 9 H, $C(CH_3)_3$); $^{13}$C NMR ($CD_3OD$, 151 MHz): $\delta = 158.6$ 158.3 (O(C=O)N O(C=O)N), 153.9

($C^{Ar}$–N=N), 144.5 ($\underline{C}^{Py}$–$CH_2$), 142.8 ($\underline{C}^{Ar}$–$CH_2$–NH), 140.8 (Me$\underline{C}^{Py}$), 136.0 ($C^{Py}$–N=N), 128.7 ($HC^{Ar}$), 123.0 ($HC^{Ar}$), 80.3, 79.9 ($\underline{C}Me_3$ $\underline{C}Me_3$), 44.8 (Ar–$CH_2$), 40.8 ($CH_2N$), 36.2 ($NCH_3$), 29.2 ($CH_2$), 28.8 28.8 (C($\underline{C}H_3$)$_3$ C($\underline{C}H_3$)$_3$), 10.0 ($CH_3$); HRMS: calcd. for $C_{24}H_{36}N_6O_4$: 473.2871 $[M+H]^+$, found: 473.2850. (*E*)-**11**: HPLC: $t_R$ = 12.467 min (65–80 % MeCN in water over 15 min); $^1$H NMR ($CD_3OD$, 600 MHz): $\delta$ = 7.76 (m, 2 H, $HC^{Ar}$), 7.39 (m, 2 H, $HC^{Ar}$), 4.30 (s, 2 H, Ar–$CH_2$N), 3.84 (s, 3 H, $NCH_3$), 3.40 (t, $J$ = 6.5 Hz, 2 H, $CH_2$–$C\underline{H}_2$N), 3.22 (t, $J$ = 6.5 Hz, 2 H, $C\underline{H}_2$–$CH_2$N), 2.46 (s, 3 H, $CH_3$), 1.48 (s, 9 H, C($CH_3$)$_3$), 1.34 (s, 9 H, C($CH_3$)$_3$); $^{13}$C NMR ($CD_3OD$, 151 MHz): $\delta$ = 158.6 158.3 (O(C=O)N O(C=O)N), 154.0 ($C^{Ar}$–N=N), 143.4 (Me$\underline{C}^{Py}$), 142.8 ($\underline{C}^{Ar}$–$CH_2$–NH), 141.6 ($\underline{C}^{Py}$–$CH_2$), 136.4 ($C^{Py}$–N=N), 128.7 ($HC^{Ar}$), 123.0 ($HC^{Ar}$), 80.3 80.1 ($\underline{C}Me_3$ $\underline{C}Me_3$), 44.8 (Ar–$CH_2$), 40.2 ($CH_2N$), 36.4 ($NCH_3$), 28.8 28.7 (C($\underline{C}H_3$)$_3$ C($\underline{C}H_3$)$_3$), 26.0 ($CH_2$), 13.7 ($CH_3$); HRMS: calcd. for $C_{24}H_{36}N_6O_4$: 473.2871 $[M+H]^+$, found: 473.2850.

**Photoglycoconjugate (*E*)-13**: In darkness, linker (*E*)-**10** (10.0 mg, 21.2 μmol) was dissolved in a mixture of dry $CH_2Cl_2$ (1.00 mL) and TFA (0.38 mL) before it was stirred for 1 h. Solvents were removed under reduced pressure followed by evaporation with dry $CH_2Cl_2$ (1.00 mL). The residue was dissolved under an $N_2$ atmosphere in dry $CH_2Cl_2$ (2.5 mL), Hünig's base (0.18 mL, 106 μmol) and carbonate **12**.[22b,29] (23.9 mg, 46.6 μmol) were added. The mixture was stirred for 3 h before all volatile compounds were removed under reduced pressure. The crude mix was then purified by FC ($CH_2Cl_2$/MeOH 12.5:1) yielding protected ligand (*E*)-**13** (16.7 mg, 77 %) as a yellow solid. LC–MS: $t_R$ = 7.929 min (30–80 % MeCN in water over 10 min); $^1$H NMR ($CDCl_3$, 600 MHz): $\delta$ = 7.83-7.73 (m, 2 H, $HC^{Ar}$), 7.53–7.38 (m, 2 H, $HC^{Ar}$), 6.16-6.09 (m, 1 H, H-1), 6.08-5.98 (m, 1 H, H-1'), 5.87–5.56 (m, 4 H, NH NH' O(C=O)NH O(C=O)NH'), 5.27–5.00 (m, 4 H, H-3 H-3' H-4 H-4'), 4.59–4.34 (m, 4 H, Ar-$CH_2$N H-2 H-2'), 4.29–3.52 (m, 11 H, H-5, H-5', H-6a, 6b, H-6a', H-6b', $CH_2$N, $NCH_3$), 3.40-3.05 (m, 2 H, $CH_2$), 2.70–2.52 (m, 3 H, $CH_3$), 2.14–1.85 (m, 24 H, 8 Ac); $^{13}$C NMR ($CDCl_3$, 151 MHz): $\delta$ = 171.8, 171.7, 171.0, 170.9, 170.14, 170.09, 169.2, 169.1 (C=O), 154.0, 153.8 (O(C=O)N), 152.9 ($C^{Ar}$–N=N), 142.9 ($\underline{C}^{Py}$–$CH_2$), 140.2 (Me$\underline{C}^{Py}$), 139.4 ($\underline{C}^{Ar}$–$CH_2$–NH), 135.2 ($C^{Py}$–N=N), 128.6 ($HC^{Ar-2}$), 122.3 ($HC^{Ar-1}$), 92.0, 91.7 (C-1 C-1'), 71.1, 70.9 (C-4 C-4'), 69.6, 69.4 (C-5 C-5'), 67.73, 67.72 (C-3 C-3'), 61.8, 61.6 (C-6 C-6'), 51.1, 50.9 (C-2 C-2'), 45.1 (Ar-$CH_2$), 40.4 ($CH_2$N), 36.3 ($NCH_3$), 29.1 ($CH_2$), 22.4, 20.7 20.6 ((C=O)$CH_3$), 9.9 ($CH_3$); HRMS: calcd. for $C_{44}H_{58}N_8O_{20}$: 1041.3660 $[M+Na]^+$, found: 1041.3624.

**Photoligand (*E*)-3**: In darkness, protected ligand (*E*)-**13** (15 mg, 14.7 μmol) was dissolved in MeOH (2 mL), and potassium carbonate (2.0 mg, 14.7 μmol) was added. The mixture was shaken for 1 h in a safety lock Eppendorf tube before it was centrifuged (Eppendorf Centrifuge MiniSpin, 10 000 rpm, 5 min) and the supernatant decanted. The residue was washed with MeOH (three times 0.5 mL) and concentrated under reduced pressure yielded ligand (*E*)-**3** (9.9 mg, 88 %) as a bright yellow powder without further purification. LC–MS: $t_R$ = 8.375 min (10–50 % MeCN in water over 10 min); $^1$H NMR ([$D_6$]DMSO, 600 MHz): $\delta$ = 7.93–7.54 (m, 5 H, NH NH' $HC^{Ar-1}$ O(C=O)NH), 7.40 (m, 2 H, $HC^{Ar-2}$), 7.27 (t, $J$ = 5.7 Hz, 1 H, O(C=O)NH'), 5.89–5.80 (m, 2 H, H-1 H-1'), 5.30–5.02 (m, 2 H, OH-4 OH-4'), 4.96-4.79 (m, 2 H, OH-3 OH-3'), 4.68–4.41 (m, 2 H, OH-6 OH-6'), 4.27 (d, $J$ = 6.0 Hz, 2 H, Ar-$CH_2$N), 3.82–3.68 (m, 5 H, H-2, H-2', $NCH_3$), 3.66–3.40 (m, 8 H, H-3, H-3', H-5, H-5', H-6ab, H-6ab'), 3.33–3.15 (m, 4 H, H-4, H-4', $CH_2$N), 2.94 (m, 2 H, $CH_2$), 2.55 (s, 3 H, $CH_3$), 1.82 (s, 6 H, $CH_3$); $^{13}$C NMR ([$D_6$]DMSO, 151 MHz): $\delta$ = 169.8 (C=O), 155.2, 154.8 (O(C=O)N), 151.9 ($C^{Ar}$-N=N), 141.5 ($\underline{C}^{Ar}$–$CH_2$–NH), 141.1 ($\underline{C}^{Py}$–$CH_2$), 139.8 ($C^{Py}$–N=N), 134.3 (Me$\underline{C}^{Py}$), 127.7 ($HC^{Ar-2}$), 121.5 ($HC^{Ar-1}$), 91.2, 91.0 (C-1, C-1'), 74.7, 74.6 (C-5, C-5'), 70.2 (C-4, C-4', C-3, C-3'), 60.5 (C-6, C-6'), 53.0 (C-2, C-2'), 43.5 (Ar–$CH_2$), 40.1 ($CH_2$N), 36.1 ($NCH_3$), 28.3 ($CH_2$), 22.6 ((C=O)$CH_3$), 9.6 ($CH_3$); HRMS: calcd. for $C_{32}H_{46}N_8O_{30}$: 767.3206 $[M+H]^+$, found: 767.3189.

**Ligand modeling**: Target structure conformations were energetically minimized by MM2 calculations of Chem3D Pro 16.0.1.4 by PerkinElmer Informatics. Superimposition models, graphics and analyses were performed with UCSF Chimera package 1.11.2 developed by the Resource for Biocomputing, Visualization, and Informatics at the University of California, San Francisco (supported by NIGMS P41-GM103311).[33]

**UV/vis spectroscopy and laser irradiation**: 3.00 mL of $1.07 \cdot 10^{-5} \pm 3 \cdot 10^{-8}$ M photoswitch compound solutions were transferred into a 3.5 mL Suprasil cuvette type 101-QS from Hellma Analytics. The solutions were illuminated by pulsed laser light of 2nd and 3rd harmonic of a Nd:YAG laser Powerlite 8000 from Continuum (FWHM 14 ns). As the wavelength either 532 nm or 355 nm was selected. Other wavelength contributions were removed by a combination of wavelength selective mirrors and filters. The beams were enlarged to a size with which the cuvettes could be illuminated homogeneously from above at 20 °C. The energy applied to the cuvette area was measured after the cuvette sized aperture before and after illumination sequences. After each illumination sequence, spectra were recorded with a scan rate of 4800 nm min$^{-1}$ by a Cary 50 spectrometer from Varian. Spectra of the PSS's were taken as well with a scan rate of 300 nm min$^{-1}$ to obtain precise values for the absorption coefficients. Data were processed with the program Origin 2017G SR 2 from OriginLab.

**ITC measurements**: Wheat germ agglutinin (lectin from *Tritium vulgaris*) was purchased from Sigma–Aldrich. Isothermal titration thermograms were measured using an $iTC_{200}$ calorimeter from Malvern. The buffer solution was prepared from 423 mg $NaH_2PO_4 \cdot H_2O$, 692 mg $Na_2HPO_4 \cdot 12H_2O$ and 372 mg KCl dissolved in 100 mL Milli-Q water, followed by adjusting the pH to 7.00, with either 1 M sodium hydroxide or 1 M HCl solution, then 5.26 mL DMSO were added to obtain a 5 % *v*/*v* DMSO buffer. To prepare WGA solutions, 0.3 mg samples of solid wheat germ agglutinin were dissolved in buffer solution within 15 min to obtain a roughly 20 mM solution. After centrifugation (Eppendorf Centrifuge MiniSpin, 10 000 rpm, 5 min) the solutions were decanted, and two aliquots of the protein solution were diluted to a suitable concentration for UV/vis absorption measurements (absorption between 0.01 and 0.2). The absorption was determined three times for both aliquots at 280 nm, and the mean value was used for concentration calculation using a theoretical extinction coefficient of 59200 L mol$^{-1}$ cm$^{-1}$ (ExPASy ProtParam tool[34]). For ligand aliquots, a suitable amount (4.33 mg) of ligand was dissolved in 25 mL of water with 5 % DMSO, before aliquots of 1 mL were taken and lyophilized. For a measurement one aliquot was dissolved in 500 μL of buffer and diluted to the 20-fold of the determined protein concentration. Irradiations were performed before the final dilution to corresponding protein concentration with either 532 nm, 280 mW, 2 min (*E* isomer) or 355 nm, 50 mW, 2 min (*Z* isomer). All following steps were performed in darkness or using a red-light source. Titrations were performed at 25 °C, 1000 rpm stirring speed, a reference power of 6 μcal s$^{-1}$ and 600 s initial delay for equilibration. 19 injections of 2 μL and a duration of 4 s each were performed with 120 s spacing between the injections. Prior to the titration, one injection of 0.4 μL was performed. The concentrations used in each experiment are given in the Supporting Information. Obtained data was processed and analyzed using Origin 7 and the iTC Data analysis plugin by Malvern. Integrations and baselines were manually corrected, and the binding curve was fitted using the built-in fitting model "one set of sites" of the software. Standard deviations were obtained from three independent experiments.

**DLS measurements**: Measurements were performed on a Zetasizer Nano ZSP from Malvern. WGA solutions were prepared, and their concentration determined as described for ITC measurements. In darkness, a twofold molar amount of ligand buffer solution was added, and the sample was filtrated through a 100 nm cutoff filter (Anotop 10 from Whatman). After an equilibration time of 300 s, five measurements with 10 runs (5 s each) and 5 s delay were performed. Refractive index and viscosity of the DMSO containing buffer solution required for calculations were measured experimentally. Data analysis was performed with the Zetasizer Software 7.12 from Malvern.

## Acknowledgements

This work was supported by the University of Konstanz and COST Action GLYCONanoProbes (CA18132). We thank Dr. Thomas Möller for help in setting up preliminary laser irradiation experiments and Professor Ulrich Steiner for providing the calculation of ITC curves of mixtures of ligands contained in the Supporting Information. Furthermore, we thank the NMR Core Facility of the University of Konstanz for providing the NMR instrumentation and Anke Friemel for assistance in NMR signal assignment. Open Access funding enabled and organized by Projekt DEAL.

## Conflict of Interest

The authors declare no conflict of interest.

## Data Availability Statement

The data that support the findings of this study are available in the supplementary material of this article.

**Keywords:** carbohydrates · lectins · multivalency · photochemistry · proteins

[1] *Essentials of Glycobiology*, 3rd ed. (Eds.: A. Varki, R. D. Cummings, J. D. Esko, P. Stanley, G. W. Hart, M. Aebi, A. G. Darvill, T. Kinoshita, N. H. Packer, J. H. Prestegard, R. L. Schnaar, P. H. Seeberger), Cold Spring Harbor Laboratory Press, New York, **2015**–**2017**.
[2] a) M. Mammen, S.-K. Choi, G. M. Whitesides, *Angew. Chem. Int. Ed.* **1998**, *37*, 2755–2794; *Angew. Chem.* **1998**, *110*, 2908–2953; b) C. Fasting, C. A. Schalley, M. Weber, O. Seitz, S. Hecht, B. Koksch, J. Dernedde, C. Graf, E.-W. Knapp, R. Haag, *Angew. Chem. Int. Ed.* **2012**, *51*, 10472–10498; *Angew. Chem.* **2012**, *124*, 10622–10650.
[3] Y. C. Lee, R. T. Lee, *Acc. Chem. Res.* **1995**, *28*, 321–327.
[4] a) J. J. Lundquist, E. J. Toone, *Chem. Rev.* **2002**, *102*, 555–578; b) Y. M. Chabre, R. Roy, *Adv. Carbohydr. Chem. Biochem.* **2010**, *63*, 165–393; c) C. S. Mahon, D. A. Fulton, *Nat. Chem.* **2014**, *6*, 665–672; d) S. Cecioni, A. Imberty, S. Vidal, *Chem. Rev.* **2015**, *115*, 525–561; e) C. Müller, G. Despras, T. K. Lindhorst, *Chem. Soc. Rev.* **2016**, *45*, 3275–3302; f) C. Ortiz Mellet, J.-F. Nierengarten, J. M. García Fernández, *J. Mater. Chem. B* **2017**, *5*, 6428–6436; g) M. González-Cuesta, C. Ortiz Mellet, J. M. García Fernández, *Chem. Commun.* **2020**, *56*, 5207–5222.
[5] a) V. Wittmann, S. Seeberger, *Angew. Chem. Int. Ed.* **2000**, *39*, 4348–4352; *Angew. Chem.* **2000**, *112*, 4508–4512; b) V. Wittmann, S. Seeberger, *Angew. Chem. Int. Ed.* **2004**, *43*, 900–903; *Angew. Chem.* **2004**, *116*, 918–921; c) O. Ramström, S. Lohmann, T. Bunyapaiboonsri, J.-M. Lehn, *Chem. Eur. J.* **2004**, *10*, 1711–1715; d) E. M. V. Johansson, E. Kolomiets, F. Rosenau, K.-E. Jaeger, T. Darbre, J.-L. Reymond, *New J. Chem.* **2007**, *31*, 1291–1299; e) J. S. Temme, M. G. Drzyzga, I. S. MacPherson, I. J. Krauss, *Chem. Eur. J.* **2013**, *19*, 17291–17295.
[6] a) V. Wittmann, R. J. Pieters, *Chem. Soc. Rev.* **2013**, *42*, 4492–4503; b) P. Zaree, J. Sastre Torano, C. A. M. de Haan, R. A. Scheltema, A. Barendregt, V. Thijssen, G. Yu, F. Flesch, R. J. Pieters, *Glycobiology* **2021**, *31*, 1490–1499; c) C. Dussouy, P.-A. Lalys, A. Cabanettes, V. Lehot, D. Deniaud, E. Gillon, V. Balloy, A. Varrot, S. G. Gouin, *Org. Biomol. Chem.* **2021**, *19*, 3234–3240.
[7] F. Pertici, N. de Mol, J. Kemmink, R. J. Pieters, *Chem. Eur. J.* **2013**, *19*, 16923–16927.
[8] W. Szymański, J. M. Beierle, H. A. V. Kistemaker, W. A. Velema, B. L. Feringa, *Chem. Rev.* **2013**, *113*, 6114–6178.
[9] a) F. Hamon, F. Djedaini-Pilard, F. Barbot, C. Len, *Tetrahedron* **2009**, *65*, 10105–10123; b) Y. Hu, R. F. Tabor, B. L. Wilkinson, *Org. Biomol. Chem.* **2015**, *13*, 2216–2225.
[10] a) C. E. Weston, R. D. Richardson, P. R. Haycock, A. J. P. White, M. J. Fuchter, *J. Am. Chem. Soc.* **2014**, *136*, 11878–11881; b) L. Stricker, M. Böckmann, T. M. Kirse, N. L. Doltsinis, B. J. Ravoo, *Chem. Eur. J.* **2018**, *24*, 8639–8647.
[11] C. E. Weston, A. Krämer, F. Colin, Ö. Yildiz, M. G. J. Baud, F.-J. Meyer-Almes, M. J. Fuchter, *ACS Infect. Dis.* **2017**, *3*, 152–161.
[12] D. Lachmann, A. Konieczny, M. Keller, B. König, *Org. Biomol. Chem.* **2019**, *17*, 2467–2478.
[13] N. N. Mafy, K. Matsuo, S. Hiruma, R. Uehara, N. Tamaoki, *J. Am. Chem. Soc.* **2020**, *142*, 1763–1767.
[14] O. Srinivas, N. Mitra, A. Surolia, N. Jayaraman, *J. Am. Chem. Soc.* **2002**, *124*, 2124–2125.
[15] O. Srinivas, N. Mitra, A. Surolia, N. Jayaraman, *Glycobiology* **2005**, *15*, 861–873.
[16] D. Ponader, S. Igde, M. Wehle, K. Märker, M. Santer, D. Bléger, L. Hartmann, *Beilstein J. Org. Chem.* **2014**, *10*, 1603–1612.
[17] a) V. Chandrasekaran, T. K. Lindhorst, *Chem. Commun.* **2012**, *48*, 7519–7521; b) V. Chandrasekaran, E. Johannes, H. Kobarg, F. D. Sönnichsen, T. K. Lindhorst, *ChemistryOpen* **2014**, *3*, 99–108.
[18] V. Chandrasekaran, K. Kolbe, F. Beiroth, T. K. Lindhorst, *Beilstein J. Org. Chem.* **2013**, *9*, 223–233.
[19] T. Weber, V. Chandrasekaran, I. Stamer, M. B. Thygesen, A. Terfort, T. K. Lindhorst, *Angew. Chem. Int. Ed.* **2014**, *53*, 14583–14586; *Angew. Chem.* **2014**, *126*, 14812–14815.
[20] G. Despras, L. Moeckl, A. Heitmann, I. Stamer, C. Braeuchle, T. K. Lindhorst, *ChemBioChem* **2019**, *20*, 2373–2382.
[21] Y. Nagata, M. M. Burger, *J. Biol. Chem.* **1974**, *249*, 3116–3122.
[22] a) C. Maierhofer, K. Rohmer, V. Wittmann, *Bioorg. Med. Chem.* **2007**, *15*, 7661–7676; b) D. Schwefel, C. Maierhofer, J. G. Beck, S. Seeberger, K. Diederichs, H. M. Möller, W. Welte, V. Wittmann, *J. Am. Chem. Soc.* **2010**, *132*, 8704–8719; c) P. Braun, B. Nägele, V. Wittmann, M. Drescher, *Angew. Chem. Int. Ed.* **2011**, *50*, 8428–8431; *Angew. Chem.* **2011**, *123*, 8579–8582; d) P. Rohse, V. Wittmann, *Chem. Eur. J.* **2016**, *22*, 9724–9733; e) S. Weickert, T. Seitz, W. K. Myers, C. R. Timmel, M. Drescher, V. Wittmann, *J. Phys. Chem. Lett.* **2018**, *9*, 6131–6135; f) P. Rohse, S. Weickert, M. Drescher, V. Wittmann, *Chem. Sci.* **2020**, *11*, 5227–5237.
[23] a) C. S. Wright, *J. Mol. Biol.* **1980**, *141*, 267–291; b) C. S. Wright, *J. Mol. Biol.* **1989**, *209*, 475–487; c) K. Harata, H. Nagahora, Y. Jigami, *Acta Crystallogr. Sect. D* **1995**, *51*, 1013–1019.
[24] a) C. S. Wright, *J. Mol. Biol.* **1984**, *178*, 91–104; b) M. Muraki, M. Ishimura, K. Harata, *Biochim. Biophys. Acta* **2002**, *1569*, 10–20.
[25] C. S. Wright, G. E. Kellogg, *Protein Sci.* **1996**, *5*, 1466–1476.
[26] A. Guarna, A. Brandi, F. De Sarlo, A. Goti, F. Pericciuoli, *J. Org. Chem.* **1988**, *53*, 2426–2429.
[27] M. J. Niphakis, B. J. Turunen, G. I. Georg, *J. Org. Chem.* **2010**, *75*, 6793–6805.
[28] S. Montalvão, T. O. Leino, P. S. Kiuru, K.-E. Lillsunde, J. Yli-Kauhaluoma, P. Tammela, *Arch. Pharm. Chem. Life Sci.* **2016**, *349*, 137–149.
[29] T. Seitz, C. Maierhofer, D. Matzner, V. Wittmann in *Carbohydrate Chemistry: Proven Synthetic Methods, Vol. 3* (Eds.: R. Roy, S. Vidal), CRC Press, Boca Raton, **2015**, pp. 215–218.
[30] P. Bortolus, S. Monti, *J. Phys. Chem.* **1979**, *83*, 648–652.
[31] T. K. Dam, C. F. Brewer in *Lectins* (Ed.: L. N. Carol), Elsevier Science, Amsterdam, **2007**, pp. 75–101.
[32] a) G. Bains, R. T. Lee, Y. C. Lee, E. Freire, *Biochemistry* **1992**, *31*, 12624–12628; b) M. Fiore, N. Berthet, A. Marra, E. Gillon, P. Dumy, A. Dondoni, A. Imberty, O. Renaudet, *Org. Biomol. Chem.* **2013**, *11*, 7113–7122.
[33] E. F. Pettersen, T. D. Goddard, C. C. Huang, G. S. Couch, D. M. Greenblatt, E. C. Meng, T. E. Ferrin, *J. Comput. Chem.* **2004**, *25*, 1605–1612.
[34] E. Gasteiger, C. Hoogland, A. Gattiker, S. Duvaud, M. R. Wilkins, R. D. Appel, A. Bairoch, in *The Proteomics Protocols Handbook* (Ed.: J. M. Walker), Humana, Totowa, **2005**, pp. 571–607.

Manuscript received: January 26, 2022
Accepted manuscript online: March 14, 2022
Version of record online: April 5, 2022